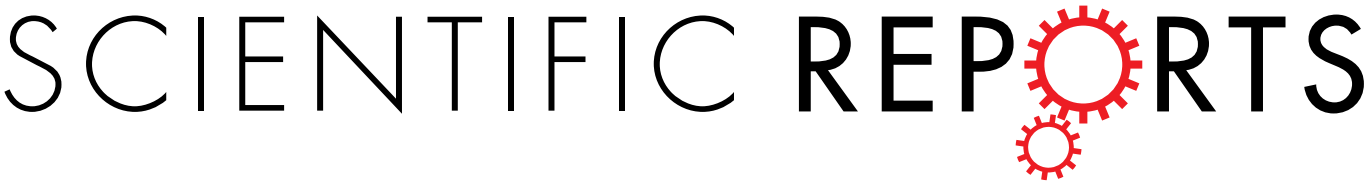

OPEN

Spin-coupling-induced Improper Polarizations and Latent Magnetization in Multiferroic $BiFeO_3$

Received: 11 October 2017
Accepted: 12 December 2017
Published online: 10 January 2018

Hyun Myung Jang[1], Hyeon Han[1] & Jung-Hoon Lee[2]

Multiferroic $BiFeO_3$ (BFO) that exhibits a gigantic off-centering polarization (OCP) is the most extensively studied material among all multiferroics. In addition to this gigantic OCP, the BFO having *R3c* structural symmetry is expected to exhibit a couple of parasitic improper polarizations owing to coexisting spin-polarization coupling mechanisms. However, these improper polarizations are not yet theoretically quantified. Herein, we show that there exist two distinct spin-coupling-induced improper polarizations in the *R3c* BFO on the basis of the Landau-Lifshitz-Ginzburg theory: ΔP_{LF} arising from the Lifshitz gradient coupling in a cycloidal spin-density wave, and ΔP_{ms} originating from the biquadratic magnetostrictive interaction. With the help of *ab initio* calculations, we have numerically evaluated magnitudes of these improper polarizations, in addition to the estimate of all three relevant coupling constants. We further predict that the magnetic susceptibility increases substantially upon the transition from the bulk *R3c* BFO to the homogeneous canted spin state in a constrained epitaxial film, which satisfactorily accounts for the experimental observation. The present study will help us understand the magnetoelectric coupling and shed light on design of BFO-based materials with improved multiferroic properties.

Multiferroics are an interesting group of materials that exhibit both ferroelectricity and anti-ferromagnetism with coupled electric and magnetic order parameters[1,2]. Multiferroism is the subject of intensive scientific investigations as these materials are able to offer a wide range of interesting applications that include sensors, transducers, memories, spintronics and ferroelectric photovoltaics[3–9]. Among numerous multiferroics, $BiFeO_3$ (BFO) is currently the only ABO_3-type simple perovskite that exhibits room-temperature multiferroism and, thus, is considered to be the most promising candidate for practical applications of multiferroics. It is a rhombohedrally distorted ferroelectric perovskite ($T_c \approx 1100\,K$) with the space group *R3c* and shows canted antiferromagnetism up to 643 K (Néel temperature, T_N)[10–12]. The *R3c* BFO is known to possess the largest reported value of the switchable polarization of ~90 $\mu C/cm^2$ along the pseudo-cubic $[111]_c$ direction (or equivalently, $[001]_h$ in hexagonal notation; Fig. 1)[13,14]. According to the previous *ab initio* studies[14–17], the stereochemically active lone-pair electrons originating from the hybridization of 6*s* and 6*p* atomic orbitals of Bi are responsible for the off-centering displacement (OCD) of the Bi ion along $[111]_c$ (or $[001]_h$). Interestingly, the *R3c* BFO is further characterized by the incommensurate cycloidal spin structure with a periodicity of 620 Å along the $[110]_h$ direction in hexagonal setting[18,19].

The magnetoelectric (ME) coupling between polarization (P) and magnetization (M) order parameters is the single most important subject of multiferroics[2]. In case of the *R3c* BFO, strong ME coupling is not anticipated due to the absence of a strong interaction between the ferroelectric OCD at the Bi-ion site and the *G*-type antiferromagnetic (AFM) spin moment at the Fe-ion site. However, the *G*-type AFM alignment plus the cycloidal spin ordering of BFO allows opportunities for interfacial magnetic coupling in multiferroic heterostructures, where BFO plays some important roles as ferroelectric substrate, AFM pinning layer for exchange bias, and interfacial quantum modulation donor[2]. Indeed, Saenrang and co-workers[20] recently demonstrated deterministic and robust

[1]Department of Materials Science and Engineering, and Division of Advanced Materials Science, Pohang University of Science and Technology (POSTECH), Pohang, 37673, Republic of Korea. [2]Department of Physics, University of California, Berkeley, Berkeley, CA, 94720-7300, USA. Correspondence and requests for materials should be addressed to H.M.J. (email: hmjang@postech.ac.kr)

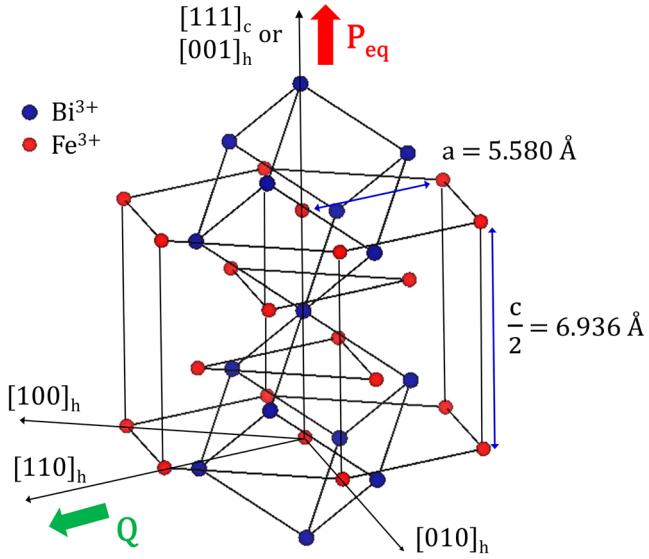

Figure 1. A half unit-cell hexagonal structure of $BiFeO_3$ having *R3c* space-group symmetry. The hexagonal lattice parameters shown in the figure ($a = b = 5.580$ Å, $c = 13.872$ Å) are based on our previous Rietveld refinement[17]. In the same figure, a pseudo-cubic representation is also shown along the $[111]_c$ direction which is equivalent to the polar $[001]_h$ direction in hexagonal notation.

room-temperature exchange coupling between the BFO AFM order and the Co overlayer with ~90° in-plane Co-moment rotation upon single-step ferroelectric switching of the monodomain BFO. This has important consequences for practical, low power non-volatile ME devices utilizing BFO[20].

In spite of extensive studies on the *R3c* BFO, however, possible ME coupling mechanisms and associated improper polarizations are not yet quantitatively resolved or lucidly explained. Herein, we show unequivocally that there exist two distinct spin-coupling-induced improper polarizations in the *R3c* BFO on the basis of the Landau-Lifshitz-Ginzburg phenomenological theory. These are: (i) a small parasitic improper polarization ($\Delta \boldsymbol{P}_{LF}$) originating from the Lifshitz exchange coupling, which can be equated with the $\boldsymbol{S}_i \times \boldsymbol{S}_j$-type vector coupling induced polarization ($\Delta \boldsymbol{P}_{DM}$) caused by the reverse Dzyaloshinskii-Moriya (DM) interaction, and (ii) a $\boldsymbol{S}_i \cdot \boldsymbol{S}_j$-type scalar coupling induced polarization ($\Delta \boldsymbol{P}_{ms}$) caused by the biquadratic magnetostrictive exchange interaction. With the help of *ab initio* density-functional theory (DFT) calculations, we have evaluated magnitudes of these improper polarizations, in addition to the numerical estimate of all three relevant ME coupling constants. We have further predicted that the magnetic susceptibility increases substantially upon the transition from the bulk *R3c* BFO to the homogeneous canted spin state in a constrained epitaxial film. These studies will help us comprehensively understand the ME coupling mechanisms in the *R3c* BFO and shed light on design of BFO-based materials with improved multiferroic properties.

Theoretical Analysis

Improper Polarization and Invariant caused by the Reverse DM Interaction. As mentioned previously, the *R3c* BFO is represented by a pseudo-cubic unit cell with its proper polarization along the cubic $[111]_c$ direction (i.e., $[001]_h$ in the hexagonal setting; Fig. 1). Let us define $[111]_c = [001]_h$ as the *z*-direction. On the other hand, the incommensurate cycloidal spin structure with a periodicity of 620 Å suggests the appearance of a small improper polarization in the *R3c* BFO *via* the reverse Dzyloshinskii-Moriya (DM) coupling[21–23]. The spin-density wave (SDW) associated with this incommensurate spin cycloid is characterized by the propagation vector $\boldsymbol{Q}$ along the $[110]_h$ direction in the hexagonal setting[18,19,24,25]. Let us define $[110]_h$ as the *x*-direction (Fig. 1). We will first examine the magnitude of this reverse DM coupling-induced parasitic polarization which is directly linked to the spin cycloid before presenting the relevant thermodynamic potential of the bulk *R3c* BFO. The induced polarization ($\Delta \boldsymbol{P}_{DM}$) by the reverse DM interaction is expressed by the following form:

$$\Delta \boldsymbol{P}_{DM} = d_{DM} \hat{\boldsymbol{e}}_{ij} \times (\boldsymbol{M}_i \times \boldsymbol{M}_j) \tag{1}$$

where $\hat{\boldsymbol{e}}_{ij}$ denotes a unit vector connecting the two neighboring magnetic (spin) moments, $\boldsymbol{M}_i$ and $\boldsymbol{M}_j$, at the sites *i* and *j*, respectively. Thus, we have to evaluate the position-dependent $(\boldsymbol{M}_i \times \boldsymbol{M}_j)$ to assess $\Delta \boldsymbol{P}_{DM}$ due to the cycloidal variation of $\boldsymbol{M}$ with the propagation vector $\boldsymbol{Q}$ along $[110]_h$.

Let us call the net magnetic moment at $x = 0$ as $\boldsymbol{M}_i$ (i.e., the site *i* at $x = 0$). Then, $\boldsymbol{M}_i$ is given by the sum of the two neighboring canted sublattice magnetization vectors, $\boldsymbol{m}_1$ and $\boldsymbol{m}_2$, along the *z*-direction (but at the same $x = 0$). Since the two neighboring canted magnetizations exhibit a canted antiferromagnetic (AFM) coupling along the *c*-axis (i.e., along $[001]_h$) with the canting angle φ, $\boldsymbol{m}_1$ and $\boldsymbol{m}_2$ can explicitly be written as $\boldsymbol{m}_1 = m_o(\cos\varphi\,\hat{\boldsymbol{z}} + \sin\varphi\,\hat{\boldsymbol{x}}) + m_y\hat{\boldsymbol{y}}$ and $\boldsymbol{m}_2 = m_o(-\cos\varphi\,\hat{\boldsymbol{z}} + \sin\varphi\hat{\boldsymbol{x}}) + m_y\hat{\boldsymbol{y}}$, where m_o denotes the magnitude of $\boldsymbol{m}_1$

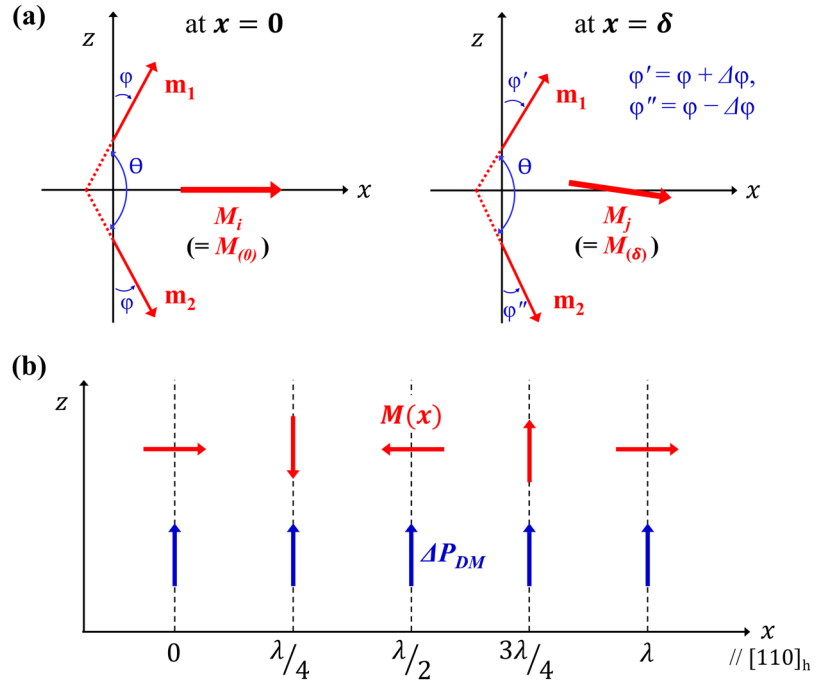

Figure 2. Canted sublattice magnetization vectors and associated polarization in the *R3c* BFO. (**a**) Two sublattice magnetization vectors, $\boldsymbol{m_1}$ and $\boldsymbol{m_2}$, at $x = 0$ (left-hand side) and at $x = \delta$ (right-hand side), projected on the hexagonal x-z plane. The figure shows $\Delta\varphi$-degree clockwise rotation of $\boldsymbol{m_1}$ or $\boldsymbol{m_2}$, as the cycloidal spin-density wave (SDW) proceeds from $x = 0$ to $x = \delta$ along the $[110]_h$ SDW propagation axis. (**b**) Cycloidal variation of $\boldsymbol{M}(\boldsymbol{x})$ along $[110]_h$. In contrast, the improper polarization caused by the reverse DM interaction, $\Delta\boldsymbol{P}_{DM}$, does uniformly polarize along the z-axis and is x-location-independent. Here, the x-axis is parallel to $[110]_h$ and the polar z-axis is parallel to $[001]_h$ or equivalently to $[111]_c$. Thus, the y-axis is parallel to $[1\bar{1}0]_h$.

(or $\boldsymbol{m_2}$) vector projected on the x-z plane (Fig. 2) and m_y designates the y-component of canted spin moment with its magnitude given by $m_y = m_o \sin\chi = m_o \sin(0.203°) = 0.0035 m_o$[17]. Thus, $\boldsymbol{M_i}$ ($\equiv \boldsymbol{M}(0)$) is given by

$$\boldsymbol{M_i} = 2m_o \sin\varphi\,\hat{\boldsymbol{x}} + 2m_y\hat{\boldsymbol{y}} \tag{2}$$

On the other hand, the two neighboring canted magnetizations, $\boldsymbol{m_1}$ and $\boldsymbol{m_2}$, at the site j, that are δ away from $x = 0$ are given by $\boldsymbol{m}_1 = m_o(\cos\varphi'\hat{\boldsymbol{z}} + \sin\varphi'\hat{\boldsymbol{x}}) + m_y\hat{\boldsymbol{y}}$ and $\boldsymbol{m}_2 = m_o(-\cos\varphi''\hat{\boldsymbol{z}} + \sin\varphi''\hat{\boldsymbol{x}}) + m_y\hat{\boldsymbol{y}}$, where $\varphi' \equiv \varphi + \Delta\varphi$ and $\varphi'' \equiv \varphi - \Delta\varphi$ with the variation of the spin-canting angle ($\Delta\varphi$) associated with the translation from $x = 0$ to $x = \delta$ along $[110]_h$. Thus, $\boldsymbol{M_j}[\equiv \boldsymbol{M}(\delta)]$ is given by $\boldsymbol{M_j} = m_o\{\sin\varphi' + \sin\varphi''\}\,\hat{\boldsymbol{x}} + m_o\{\cos\varphi' - \cos\varphi''\}\,\hat{\boldsymbol{z}} + 2m_y\hat{\boldsymbol{y}}$. This expression is readily transformed into the following form using elementary trigonometric algebra:

$$\boldsymbol{M_j} = 2m_o \sin\varphi\cos(\Delta\varphi)\hat{\boldsymbol{x}} - 2m_o \sin\varphi \sin(\Delta\varphi)\hat{\boldsymbol{z}} + 2m_y\hat{\boldsymbol{y}} \tag{3}$$

Plugging Eqs (2) and (3) into Eq. (1) yields the following expression for the improper polarization induced by the reverse DM coupling:

$$\begin{aligned}\Delta\boldsymbol{P}_{DM} &= 4m_o^2 d_{DM}\sin^2\varphi\,\sin(\Delta\varphi)\hat{\boldsymbol{z}} - 4m_o m_y \sin\varphi\{1 - \cos(\Delta\varphi)\}\hat{\boldsymbol{y}} \\ &= m_o^2 \sin\varphi[4d_{DM}\sin\varphi\sin(\Delta\varphi)\hat{\boldsymbol{z}} - 0.014\{1 - \cos(\Delta\varphi)\}\hat{\boldsymbol{y}}] \\ &\approx 4m_o^2 d_{DM}\sin^2\varphi\sin(\Delta\varphi)\hat{\boldsymbol{z}}\end{aligned} \tag{4}$$

The last expression of $\boldsymbol{P}_{DM}$ is valid if $\cos(\Delta\varphi) \approx 1$. As defined previously, $\Delta\varphi$ denotes the variation of the spin-canting angle associated with the translation from one Fe-site to the nearest-neighbor Fe-site along the x-axis. Thus, $\Delta\varphi = 360° \times (5.58\,\text{Å}/620\,\text{Å}) = 3.24°$, where 5.58 Å does correspond to the distance between the two nearest-neighbor Fe ions along the x-axis[17]. This predicts that $\cos(\Delta\varphi) = 0.9984 \approx 1$ and supports the validity of the last expression in Eq. (4). We will quantitatively examine the validity of this proposition of ignoring the y-component of the reverse DM coupling induced polarization in 'Discussion' section. It is interesting to notice that $\boldsymbol{P}_{DM}$ is location-independent but depends on the DM coupling strength (d_{DM}), canting angle (φ), and the periodicity of SDW through $\Delta\varphi$. Thus, the improper polarization induced by the reverse DM coupling does uniformly polarizes along the z-axis, i.e., along $[001]_h$ [Fig. 2].

Within a continuum approximation for magnetic properties, the DM interaction responsible for this cycloidal modulation of spin moments in the *R3c* BFO can be expressed by inhomogeneous invariants, so-called 'Lifshitz

invariants' in the free-energy density[26]. Since the leading terms in the DM interaction are linear with respect to first spatial derivatives of magnetization in an antisymmetric mathematical form, the Lifshitz invariant for the *R3c* BFO can be written as

$$\begin{aligned}\Delta f_{LF} &= \gamma_s P_z\left(L_z\frac{\partial L_x}{\partial x} - L_x\frac{\partial L_z}{\partial x}\right) + \gamma'_s P_x\left(L_x\frac{\partial L_z}{\partial z} - L_z\frac{\partial L_x}{\partial z}\right)\\ &\quad + \frac{1}{2}\kappa_s\left\{\left(\frac{\partial L_x}{\partial x}\right)^2 + \left(\frac{\partial L_z}{\partial x}\right)^2 + \left(\frac{\partial L_x}{\partial z}\right)^2 + \left(\frac{\partial L_z}{\partial z}\right)^2\right\}\end{aligned} \tag{5}$$

where γ_s and γ'_s denote the Lifshitz relativistic *P*-*L* exchange-coupling constants. Since the *R3c* BFO is antiferromagnetic (AFM), we used the magnitude of the AFM Néel vector, *L*, instead of the net magnetization order parameter, *M*, [$\equiv|\boldsymbol{m_1} + \boldsymbol{m_2}|$], in the description of Δf_{LF}. Herein, the DM vector is replaced by $\gamma_s P$ since the polarization couples to gradients of *M* or *L*, thereby inducing an inhomogeneous cycloidal spin configuration. In the next section, we will use this form of Δf_{LF} in constructing the thermodynamic potential for the *R3c* BFO.

Landau-Lifshitz-Ginzburg Thermodynamic Potential. Before presenting the free-energy density of the multiferroic *R3c* $BiFeO_3$ (BFO), we have first examined the free-energy density of the ferroelectric subsystem, $\Delta f(P)$, on the basis of Landau-Ginzburg-Devonshire phenomenological theory[27–29]. As mentioned previously, the *R3c* BFO is represented by a pseudo-cubic unit cell with its proper polarization along the cubic $[111]_c$ direction (i.e., $[001]_h$ in the hexagonal setting; Fig. 1). Then, the free-energy density (thermodynamic potential) of the ferroelectric subsystem can be expanded on the basis of a paraelectric prototypic cell having cubic $P_{m\bar{3}m}$ symmetry:

$$\Delta f(P) = f_o + \frac{1}{2}\chi_p\left(P_x^2 + P_y^2 + P_z^2\right) + \xi'_p\left(P_x^4 + P_y^4 + P_z^4\right) + \xi''_p\left(P_x^2P_y^2 + P_y^2P_z^2 + P_z^2P_x^2\right) \tag{6}$$

where χ_p denotes the dielectric stiffness, and ξ'_p, ξ''_p are high-order stiffness coefficients. In Eq. (6), the three polarization components along the three orthogonal cubic directions are denoted by P_x,P_y, and P_z. Then, the proper ferroelectric polarization (*P*) along the pseudo-cubic $[111]_c$ is given by $P^2 = P_x^2 + P_y^2 + P_z^2$. Substituting this relation into Eq. (6) and suitably rearranging the resulting relation, one can obtain the following relation:

$$\Delta f(P) = f_o + \frac{1}{2}\chi_p P^2 + \xi'_p P^4 + \xi'''_p\left(P_x^2P_y^2 + P_y^2P_z^2 + P_z^2P_x^2\right) \tag{7}$$

where ξ'''_p is defined by $\xi'''_p \equiv \xi''_p - 2\xi'_p$. Since *P* is parallel to $[111]_c$, $P_x = P_y = P_z = \frac{1}{\sqrt{3}}P$. Substituting this relation into Eq. (7), one can immediately obtain the following expression:

$$\Delta f(P) = f_o + \frac{1}{2}\chi_p P^2 + \frac{1}{4}\xi_p P^4 \tag{8}$$

where ξ_p is defined by $\xi_p \equiv \frac{4}{3}\left(3\xi'_p + \xi'''_p\right) > 0$.

Considering the Lifshitz invariant for the cycloidal modulation of spin moments [Eq. (5)] and the free-energy density for the ferroelectric subsystem [Eq. (8)], one can write down the Landau-Lifshitz-Ginzburg thermodynamic potential of the single crystalline *R3c* BFO in terms of two independent order parameters, *P* and *L*, where *L* is an AFM Néel vector describing the staggered sublattice magnetization. The model free-energy density (Δf) with respect to the paraphrase where $\langle P\rangle = \langle L\rangle = 0$ is

$$\begin{aligned}\Delta f(P,\ L) &= \frac{1}{2}\chi_p P^2 + \frac{1}{4}\xi_p P^4 + \frac{1}{2}\chi_l L^2 + \frac{1}{4}\xi_l L^4 - \gamma_q P^2(\boldsymbol{m_1}\cdot\boldsymbol{m_2}) + \frac{1}{2}\kappa_G\sum_{i=x,y,z}(\boldsymbol{\nabla}L_i)^2\\ &\quad + \gamma_s P_z\left(L_z\frac{\partial L_x}{\partial x} - L_x\frac{\partial L_z}{\partial x}\right) + \gamma'_s P_x\left(L_x\frac{\partial L_z}{\partial z} - L_z\frac{\partial L_x}{\partial z}\right)\\ &\quad + \frac{1}{2}\kappa_s\left\{\left(\frac{\partial L_x}{\partial x}\right)^2 + \left(\frac{\partial L_z}{\partial x}\right)^2 + \left(\frac{\partial L_x}{\partial z}\right)^2 + \left(\frac{\partial L_z}{\partial z}\right)^2\right\}\end{aligned} \tag{9}$$

where *P* denotes the magnitude of the total ferroelectric polarization (proper + improper) developed along the hexagonal *c*-axis, *i.e.*, $[001]_h$, or, equivalently, along $[111]_c$ of the pseudo-cubic unit cell (Fig. 1)[13,14]. According to our Berry-phase calculations, $P \approx P_z$ and P_z is as high as ~90 $\mu C/cm^2$ for the undoped BFO having the *R3c* space-group symmetry[17], where P_z designates the proper off-centering polarization developed along the hexagonal [001] direction. Here, we would like to remind that '*z*' does not refer to the cubic [001] direction. In addition, $P_x = 0$ as the SDW-propagation direction (***Q***) is parallel to *x* [Fig. 3]. Equation (4) formally supports this conclusion. Several previous investigators adopted similar forms of the free-energy density in their theoretical analysis of the *R3c* BFO[24,30–32]. However, the present form [Eq. (9)] is best suited to theoretical treatment of the spin-coupling-induced improper polarizations and the latent magnetization that are the two main subjects of the present study. The magnitude of the AFM Néel vector, *L*, is defined as $L = |\boldsymbol{m_1} - \boldsymbol{m_2}|$, where $\boldsymbol{m_1}$ and $\boldsymbol{m_2}$ denote two canted neighboring sublattice magnetization vectors[24]. Then, it can be shown immediately that *M* and *L* are

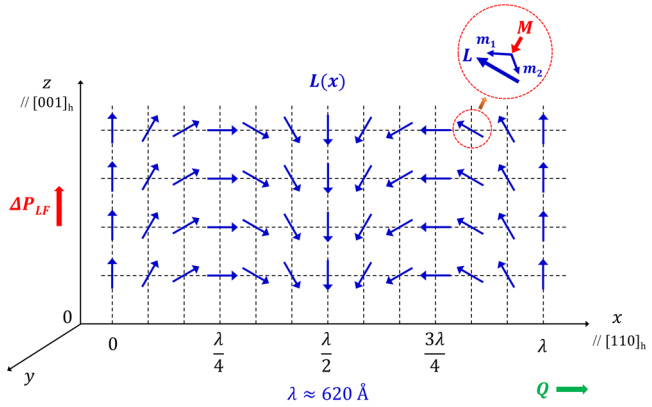

Figure 3. A two dimensional representation of the AFM Néel vector, $\boldsymbol{L}(\boldsymbol{x})$, that forms a continuously varying SDW with the propagation vector $\boldsymbol{Q}$ along the $[110]_h$. Herein, the improper polarization arising from the Lifshitz exchange coupling in the SDW is denoted by $\Delta \boldsymbol{P}_{LF}$ and is predicted to be parallel to the z-axis or $[001]_h$.

not independent of each other but are interrelated by $M^2 - L^2 = 4(\boldsymbol{m_1} \cdot \boldsymbol{m_2})$. Thus, the magnetostrictive coupling invariant in Eq. (9) can be rewritten using the following biquadratic form:

$$\Delta f_{ms} \left(\equiv \Delta f_q\right) = -\gamma_q P^2(\boldsymbol{m_1} \cdot \boldsymbol{m_2}) = -\frac{1}{4}\gamma_q P^2(M^2 - L^2).$$

Lifshitz Invariant associated with Cycloidal Spin-density Wave. As described previously, the single crystalline *R3c* BFO is characterized by the incommensurate SDW with the propagation vector $\boldsymbol{Q}$ along the $[110]_h$ spiral direction in hexagonal setting[18,19,24]. As schematically shown in Fig. 3, the x-location-dependent Néel vector $[\boldsymbol{L}(x)]$ forms a continuously varying cycloidal vector on the x-z plane with its propagation direction $\boldsymbol{Q}$ along $\hat{\boldsymbol{x}}$ $(=[110]_h)$. Thus, the Néel vector is given by $\boldsymbol{L}(x) = L_x\hat{\boldsymbol{x}} + L_z\hat{\boldsymbol{z}}$. Since the Néel vector $\boldsymbol{L}(x)$ lies on the x-z plane, $L_y = 0$. Accordingly, we establish the following expressions for two orthogonal components of $\boldsymbol{L}(x)$:

$$L_x = L_o \sin(Qx) \text{ and } L_z = L_o \cos(Qx) \tag{10}$$

where $Q \equiv |\boldsymbol{Q}| = 2\pi/\lambda$ with $\lambda = 620$ Å. One can readily obtain the following relations for M_x and M_z from Eq. (10): $M_x = M_o\cos(Qx)$ and $M_z = -M_o\sin(Qx)$. Thus, $\boldsymbol{M}(x)$ and $\boldsymbol{L}(x)$ vectors are perpendicular to each other.

Let us then find a Lifshitz invariant arising from this cycloidal SDW. One can compactly rewrite the Lifshitz invariant by assuming that $\gamma_s = \gamma_s'$ for simplicity.

$$\begin{aligned}\Delta f_{LF} &= \gamma_s \boldsymbol{P} \cdot \{\boldsymbol{L}(\boldsymbol{\nabla} \cdot \boldsymbol{L}) - (\boldsymbol{L} \cdot \boldsymbol{\nabla})\boldsymbol{L}\} + \frac{1}{2}k_s\{(\nabla_x L_x)^2 + (\nabla_x L_z)^2 + (\nabla_z L_x)^2 + (\nabla_z L_z)^2\} \\ &\approx \gamma_s \boldsymbol{P} \cdot \{\boldsymbol{L}(\boldsymbol{\nabla} \cdot \boldsymbol{L}) - (\boldsymbol{L} \cdot \boldsymbol{\nabla})\boldsymbol{L}\}\end{aligned} \tag{11}$$

In obtaining the last expression, we omitted terms representing the square of Néel-vector gradients. According to Mostovoy[33], these nonlinear square terms do not practically contribute to the uniform improper polarization caused by the Lifshitz P-L exchange coupling. Since $\boldsymbol{L}(x) = L_x\hat{\boldsymbol{x}} + L_z\hat{\boldsymbol{z}}$, it can be shown that the Lifshitz invariant is given by

$$\begin{aligned}\Delta f_{LF} &\approx \gamma_s\{P_x\hat{\boldsymbol{x}} + P_y\hat{\boldsymbol{y}} + P_z\hat{\boldsymbol{z}}\} \cdot \left\{\left(L_x\frac{\partial L_z}{\partial z} - L_z\frac{\partial L_x}{\partial z}\right)\hat{\boldsymbol{x}} + \left(L_z\frac{\partial L_x}{\partial x} - L_x\frac{\partial L_z}{\partial x}\right)\hat{\boldsymbol{z}}\right\} \\ &= \gamma_s P_z\left(L_z\frac{\partial L_x}{\partial x} - L_x\frac{\partial L_z}{\partial x}\right)\end{aligned} \tag{12}$$

In obtaining the last expression, we used the equality that $\frac{\partial L_z}{\partial z} = \frac{\partial L_x}{\partial z} = 0$ since both L_x and L_z are independent of the z-coordinate [Fig. 3] and that $P_x = 0$ as the SDW-propagation direction ($\boldsymbol{Q}$) is parallel to x. Combining this result with the two relations given in Eq. (10), one can obtain the following expression of the Lifshitz invariant:

$$\Delta f_{LF} = \gamma_s P_z L_o^2 \{\cos^2(Qx) + \sin^2(Qx)\}Q = \gamma_s P_z L_o^2 Q \tag{13}$$

where $L_o (\equiv L = |\boldsymbol{m_1} - \boldsymbol{m_2}|)$ denotes the magnitude of Néel vector and is given by $L_o^2 = 4m_o^2\cos^2\varphi \approx 4m_o^2$ since $\varphi \approx 0.7°$ [Fig. 2].

R. de Sousa and J. E. Moore[24] used another form of the Lifshitz exchange coupling for the *R3c* BFO, which is apparently different from Δf_{LF} presented in Eq. (11). It is given by

$$\Delta f'_{LF} = \gamma_s \boldsymbol{P} \cdot \{\boldsymbol{L}(\boldsymbol{\nabla} \cdot \boldsymbol{L}) + \boldsymbol{L} \times (\boldsymbol{\nabla} \times \boldsymbol{L})\} \tag{14}$$

After carrying out several steps for mathematical rearrangements, one can show that

$$\Delta f'_{LF} = \gamma_s\left[\left\{P_xL_x\left(\frac{\partial L_x}{\partial x}\right) + P_xL_z\left(\frac{\partial L_z}{\partial x}\right)\right\} + \left\{P_zL_z\left(\frac{\partial L_x}{\partial x}\right) - P_zL_x\left(\frac{\partial L_z}{\partial x}\right)\right\}\right] \tag{15}$$

In obtaining the above relation, we used the equality that $\left(\frac{\partial L_x}{\partial y}\right) = \left(\frac{\partial L_x}{\partial z}\right) = \left(\frac{\partial L_z}{\partial y}\right) = 0$. As mentioned previously, $P_x = 0$ since the SDW-propagation direction ($\mathbf{Q}$) is parallel to x. Then, combining Eq. (15) with Eq. (10) immediately yields

$$\Delta f'_{LF} = \gamma_s P_z\left(L_z\frac{\partial L_x}{\partial x} - L_x\frac{\partial L_z}{\partial x}\right) = \gamma_s P_z\, L_o^2\, Q \tag{16}$$

Accordingly, $\Delta f_{LF} = \Delta f'_{LF}$. This indicates that the two apparently different forms of the Lifshitz invariant [i.e., Eqs (11) and (14)] are equal to each other under the condition of cycloidal spin ordering confined in an x-z plane with the translational symmetry along $\hat{\boldsymbol{y}}$ and the propagation direction along $\hat{\boldsymbol{x}}$ which is parallel to $[110]_h$.

Free-energy Minimization for Deducing Two Distinct Improper Polarizations. Incorporating the results of Eq. (13) for the Lifshitz invariant into Eq. (9), we obtain a simplified form of the thermodynamic potential.

$$\begin{aligned}\Delta f(P, L) = {} & \frac{1}{2}\chi_p P^2 + \frac{1}{4}\xi_p P^4 + \frac{1}{2}\chi_l L^2 + \frac{1}{4}\xi_l L^4 - \frac{1}{4}\gamma_q P^2(M^2 - L^2) \\ & + \frac{1}{2}\kappa_G \sum_{i=x,y,z}(\boldsymbol{\nabla} L_i)^2 + \gamma_s P L^2 Q\end{aligned} \tag{17}$$

where we used the notation P for the proper off-centering polarization, P_z, since $P_z \approx P$. Then, consider the free-energy functional for a finite volume, $\Delta F = \int dv \Delta f(P,L)$. We impose the following equality for equilibrium: $\delta\Delta F = \int dv\left\{\left(\frac{\partial \Delta f}{\partial P}\right)_L \delta P + \left(\frac{\partial \Delta f}{\partial L}\right)_P \delta L\right\} = 0$. Since the P-L cross-coupling is sufficiently weak, one can establish:

$$\int dv\ \delta P\left(\frac{\partial \Delta f}{\partial P}\right)_L = \int dv\ \delta L\left(\frac{\partial \Delta f}{\partial L}\right)_P = 0 \tag{18}$$

Let us first consider the equilibrium off-centering (proper) polarization. One can immediately establish the following equality by imposing Eq. (18) to Eq. (17):

$$\int dv\ \delta P\left\{\chi_p P + \xi_p P^3 - \frac{1}{2}\gamma_q(M^2 - L^2)P + \gamma_s L^2 Q\right\} = 0 \tag{19}$$

If the Lifshitz-coupling term were absent, one would obtain the following relation from Eq. (19): $P_o\left\{\chi_p + \xi_p P_o^2 - \frac{1}{2}\gamma_q(M^2 - L^2)\right\} = 0$. Then, one immediately obtains the following expression for the equilibrium polarization (P_o) in the absence of the Lifshitz exchange coupling:

$$P_o^2 = -\left(\frac{1}{\xi_p}\right)\left\{\chi_p - \frac{1}{2}\gamma_q(M^2 - L^2)\right\} \equiv \left(P_{eq(0)} + \Delta P_{ms}\right)^2 \tag{20}$$

where $P_{eq(0)}$ denotes the equilibrium (proper) off-centering polarization in the absence of any intrinsic ME coupling and ΔP_{ms} ($\equiv|\Delta \boldsymbol{P}_{ms}|$) represents a small improper polarization caused by the magnetostrictive exchange coupling. Thus, P_o is comprised of two distinct terms, namely, $P_o = P_{eq(0)} + \Delta P_{ms}$. Since $P_{eq(0)} \gg \Delta P_{ms}$, we establish the following relations from Eq. (20):

$$(P_{eq(0)})^2 = -\left(\frac{\chi_p}{\xi_p}\right) \text{ and } \Delta P_{ms} = \frac{\gamma_q(M^2 - L^2)}{4\xi_p P_{eq(0)}} = \frac{\gamma_q(\boldsymbol{m_1}\cdot\boldsymbol{m_2})}{\xi_p P_{eq(0)}} < 0 \tag{21}$$

According to the Curie-Weiss law, $\chi_p = \frac{4\pi}{c}(T - T_c)$, where T_c denotes the ferroelectric Curie temperature ($\approx$1100 K for the $R3c$ BFO)[11,34]. Thus, $\chi_p < 0$ below T_c. Let the total equilibrium polarization that satisfies Eq. (19) be P_{eq}. We then establish

$$P_{eq} \equiv P_o + \Delta P_{LF} = \left(P_{eq(0)} + \Delta P_{ms}\right) + \Delta P_{LF} \tag{22}$$

In the above equation, ΔP_{LF} ($\equiv|\Delta \boldsymbol{P}_{LF}|$) appears due to the last term in the parenthesis of Eq. (19) and thus represents a small improper polarization arising from the Lifshitz coupling.

Owing to the Lifshitz invariant, one cannot obtain a correct analytic solution of P_{eq} from Eq. (19). We thus treat ΔP_{LF} as a small perturbation to P_o and obtain a reasonably accurate solution for ΔP_{LF}. Substituting Eq. (22) into Eq. (19) yields the following equality:

$$\left\{\chi_p P_o + \xi_p P_o^3 - \frac{1}{2}\gamma_q(M^2 - L^2)P_o\right\}$$
$$+\chi_p \Delta P_{LF} + \xi_p\{3P_o^2\Delta P_{LF} + 3P_o(\Delta P_{LF})^2\}$$
$$-\frac{1}{2}\gamma_q(M^2 - L^2)\Delta P_{LF} + \gamma_s L_o^2 Q = 0 \tag{23}$$

As discussed previously, the terms inside the first parenthesis are equal to 0. Neglecting the term containing $(\Delta P_{LF})^2$, we eventually derive the following expressions of ΔP_{LF}:

$$\Delta P_{LF} = \frac{-\gamma_s L_o^2 Q}{\left\{-2\chi_p + \gamma_q(M^2 - L^2)\right\}} = \frac{-\gamma_s L_o^2 Q}{2\xi_p P_o^2} > 0 \tag{24}$$

In obtaining the second expression of Eq. (24), we substitute Eq. (20) for P_o^2. On the other hand, we used the following equality in obtaining the last relation: $\chi_p + \xi_p P_o^2 - \frac{1}{2}\gamma_q(M^2 - L^2) = 0$. This equality was previously discussed in conjunction with Eq. (19).

On the other hand, the improper polarization caused by the magnetostrictive exchange coupling (ΔP_{ms}) is given in Eq. (21). Let us now rewrite ΔP_{ms} in terms of L_o^2 to compare this with ΔP_{LF}. The term, $\boldsymbol{m_1}\cdot\boldsymbol{m_2}$, appeared in Eq. (21) can be rewritten in terms of the AFM spin angle θ as $\boldsymbol{m_1}\cdot\boldsymbol{m_2} \approx m_o^2\cos\theta = -m_o^2|\cos\theta| = -m_o^2|\cos(178.6^\circ)| < 0$. In addition to this, $P_o = P_{eq(0)} + \Delta P_{ms} \approx P_{eq(0)}$, and $|\boldsymbol{L}| \equiv |\boldsymbol{m_1} - \boldsymbol{m_2}| = L_o = 2m_o\cos\varphi = 2m_o\cos(0.7^\circ) \approx 2m_o$, where $\theta + 2\varphi = 180^\circ$ [Fig. 2(a)]. Incorporating these three results into Eq. (21), one immediately obtains

$$\Delta P_{ms} = \frac{-\gamma_q L_o^2|\cos\theta|}{4\xi_p P_o} \approx \frac{-\gamma_q m_o^2}{\xi_p P_o} < 0 \tag{25}$$

The above equation demonstrates that the improper polarization caused by the magnetostrictive interaction belongs to $\boldsymbol{S}_i\cdot\boldsymbol{S}_j$-type scalar coupling. According to Eq. (25), $|\Delta P_{ms}|$ is inversely proportional to P_o. In contrast, $|\Delta P_{LF}|$ is inversely proportional to the square of P_o. Since $|\cos\theta| \approx 1$, the ratio of these two antiparallel improper polarizations is obtained from Eqs (24) and (25), namely, $\frac{|\Delta P_{LF}|}{|\Delta P_{ms}|} = \frac{2|\gamma_s|Q}{\gamma_q P_o} = \frac{4\pi|\gamma_s|}{\gamma_q P_o \lambda}$. Finally, the corresponding coupling invariant (Δf_{ms}) can be obtained by using the relation described previously, $\boldsymbol{m_1}\cdot\boldsymbol{m_2} = -m_o^2|\cos\theta|$.

$$\Delta f_{ms}\left(\equiv\Delta f_q\right) = -\frac{1}{4}\gamma_q P^2(M^2 - L^2) = -\gamma_q P^2(\boldsymbol{m_1}\cdot\boldsymbol{m_2}) = +\gamma_q P^2 m_o^2|\cos\theta| \tag{26}$$

where P is nearly equal to P_z or P_o. The subscript 'q' appeared in Δf_q emphasizes that the magnetostrictive interaction is represented by a biquadratic coupling of the form, P^2M^2 or P^2L^2. According to ϕ^4-expansion adopted in Eq. (8) [or Eq. (17)], the Landau coefficient ξ_p should be positive. Thus, Eq. (26) tells us that the biquadratic P-M cross-coupling thermodynamically stabilizes the *R3c* BFO system if $\gamma_q < 0$. On the contrary, the biquadratic magnetostrictive coupling destabilizes the system with a concomitant decrease in P_o (i.e., $\Delta P_{ms} < 0$) if $\gamma_q > 0$. According to the experimental result reported by S. Lee *et al.*[25], the latter case ($\gamma_q > 0$) is applicable to the *R3c* BFO. Our theoretical estimate also supports this conclusion ('Discussion' section).

Since ΔP_{LF} appeared in Eq. (24) is equal to $|\Delta \boldsymbol{P}_{DM}|$ that is given in Eq. (4), one can derive the following analytical expression for the reverse DM interaction coefficient (d_{DM}) which is a measure of the strength of the reverse DM coupling:

$$d_{DM} = \frac{\pi|\gamma_s|}{\lambda\xi_p \sin(\Delta\varphi)\tan^2\varphi P_o^2} \tag{27}$$

As expected, d_{DM} is proportional to the Lifshitz P-L exchange-coupling constant ($|\gamma_s|$) but is inversely proportional to λ (wavelength of the SDW, 620 Å along the $[110]_h$). To estimate d_{DM}, thus, one should first know γ_s, ξ_p, and P_o. We will show all the details in 'Discussion' section.

Ginzburg Gradient Energy and Equilibrium Magnetic Remanence. Let us examine the second relation of Eq. (18) by applying Eq. (17) to this requirement.

$$\int dv\ \delta L\left(\frac{\partial\Delta f}{\partial L}\right)_P = \int dv\ \delta L\left[\chi_l L + \xi_l L^3 + \frac{1}{2}\gamma_q P^2 L + 2\gamma_s PQL + \frac{1}{2}\kappa_G\frac{\partial\{\sum_i(\nabla \boldsymbol{L}_i)^2\}}{\partial L}\right] = 0 \tag{28}$$

where κ_G denotes the Ginzburg gradient-energy coefficient. The last term inside the parenthesis of Eq. (28) can be rewritten as

$$\frac{1}{2}\kappa_G\frac{\partial\{\sum_i(\nabla \boldsymbol{L}_i)^2\}}{\partial L} = \frac{1}{2}\kappa_G\frac{\partial\{\sum_i(\nabla \boldsymbol{L}_i)^2\}}{\partial L_i}\frac{\partial L_i}{\partial L} = -\kappa_G\sum_i \nabla^2 L_i\left(\frac{\partial L_i}{\partial L}\right)_{L_j} \tag{29}$$

Then, we obtain the following type Euler-Lagrange equation from Eq. (28):

$$L\left\{\chi_l + \xi_l L^2 + \frac{1}{2}\gamma_q P^2 + 2\gamma_s PQ\right\} - \kappa_G \sum_i \nabla^2 L_i \left(\frac{\partial L_i}{\partial L}\right)_{L_j} = 0 \tag{30}$$

The Ginzburg gradient term in the above equation is comprised of three distinct terms, namely,

$$-\kappa_G \sum_i \nabla^2 L_i \left(\frac{\partial L_i}{\partial L}\right)_{L_j} = -\kappa_G \left\{ \nabla^2 L_x \left(\frac{\partial L_x}{\partial L}\right)_{L_y,L_z} + \nabla^2 L_y \left(\frac{\partial L_y}{\partial L}\right)_{L_x,L_z} + \nabla^2 L_z \left(\frac{\partial L_z}{\partial L}\right)_{L_x,L_y} \right\} \tag{31}$$

Since $\nabla^2 L_x = \boldsymbol{\nabla}\cdot\boldsymbol{\nabla} L_x$ and $\frac{\partial L_x}{\partial y} = \frac{\partial L_x}{\partial z} = 0$, it is not difficult to show that $\nabla^2 L_x = -L_o Q^2 \sin(Qx)$, where L_o denotes the magnitude of the AFM Néel vector. Similarly, it can be shown readily that $\nabla^2 L_z = \boldsymbol{\nabla}\cdot\boldsymbol{\nabla} L_z = -L_o Q^2 \cos(Qx)$. On the contrary, $\nabla^2 L_y = \boldsymbol{\nabla}\cdot\boldsymbol{\nabla} L_y = 0$. In addition, it is straightforward to show $\left(\frac{\partial L_x}{\partial L}\right)_{L_y,L_z} = \frac{L_o}{L_x} = \frac{1}{\sin(Qx)}$ and $\left(\frac{\partial L_z}{\partial L}\right)_{L_x,L_y} = \frac{L_o}{L_z} = \frac{1}{\cos(Qx)}$. Putting all these results into Eq. (31) and rearranging yields to the following expression for the Ginzburg gradient term:

$$+\frac{1}{2}\kappa_G \frac{\partial\{\sum_i (\nabla \boldsymbol{L}_i)^2\}}{\partial L} = -\kappa_G \sum_i \nabla^2 L_i \left(\frac{\partial L_i}{\partial L}\right)_{L_j} = +2\kappa_G L_o Q^2 \tag{32}$$

where $L = L_o$. Substituting Eq. (32) into Eq. (28) yields the following expression for the equilibrium magnitude of the AFM Néel vector:

$$\left(L_{eq}\right)^2 = \left(L_{eq(0)}\right)^2 - \frac{\left\{\frac{1}{2}\gamma_q P^2 + 2\gamma_s PQ + 2\kappa_G Q^2\right\}}{\xi_l} \tag{33}$$

where $\left(L_{eq(0)}\right)^2 \equiv -\chi_l/\xi_l$. Thus, $L_{eq(0)}$ denotes the equilibrium magnitude of the Néel vector in the absence of any coupling (*i.e.*, $\gamma_q = \gamma_s = \kappa_G = 0$). Then, the equilibrium magnetic remanence (M_{eq}) is related to L_{eq} *via* the following relation: $\left(M_{eq}\right)^2 = \left(L_{eq}\right)^2 + 4(\boldsymbol{m_1}\cdot\boldsymbol{m_2})_{eq}$. Combining this relation with Eq. (33) yields

$$\left(M_{eq}\right)^2 = \left(M_{eq(0)}\right)^2 + 4\delta(\boldsymbol{m_1}\cdot\boldsymbol{m_2})_{eq} - \frac{\left\{\frac{1}{2}\gamma_q P^2 + 2\gamma_s PQ + 2\kappa_G Q^2\right\}}{\xi_l} \tag{34}$$

where $\delta(\boldsymbol{m_1}\cdot\boldsymbol{m_2})_{eq} \equiv (\boldsymbol{m_1}\cdot\boldsymbol{m_2})_{eq} - (\boldsymbol{m_1}\cdot\boldsymbol{m_2})_{eq(0)}$ and $M_{eq(0)}$ denotes the equilibrium magnetic remanence in the absence of any coupling. Thus, the Lifshitz exchange coupling enhances M_{eq} if $\gamma_s < 0$ which corresponds to thermodynamically favorable Lifshitz coupling [Eq. (13)]. According to our theoretical estimate, γ_s is indeed negative as described in 'Discussion' section. In contrast, the Ginzburg gradient term always suppresses M_{eq} as $\kappa_G > 0$.

The Ginzburg gradient energy can be computed by considering the space average of the gradient term in Eq. (17), namely, $\Delta f_G = \frac{1}{2}\kappa_G\langle\sum_i(\nabla L_i)^2\rangle = \frac{1}{2}\kappa_G\langle(\nabla L_x)^2 + \left(\nabla L_y\right)^2 + (\nabla L_z)^2\rangle$. It can be shown readily that $(\nabla L_x)^2 = (\nabla L_x)\cdot(\nabla L_x) = L_o^2 Q^2\cos^2(Qx)$ and $(\nabla L_z)^2 = L_o^2 Q^2 \sin^2(Qx)$. On the contrary, $(\nabla L_y)^2 = 0$ since $L_y = 0$. Thus, the space average of the Ginzburg gradient term is

$$\Delta f_G = \frac{1}{2}\kappa_G \left\langle \sum_i (\nabla L_i)^2 \right\rangle = \frac{1}{2}\kappa_G L_o^2 Q^2 \tag{35}$$

Since $\kappa_G > 0$, the Ginzburg gradient term always increases the free-energy density.

Discussion

Estimate of the Two distinct Improper Polarizations. Having theoretically identified the two spin-coupling-induced improper polarizations in the *R3c* BFO (i.e., ΔP_{ms}, ΔP_{LF}), we now focus on the numerical estimate of these values with the help of *ab initio* density-functional theory (DFT) calculations and experimental measurements. For this, let us first consider the improper polarization caused by the magnetostrictive exchange coupling, ΔP_{ms}. As given in Eq. (20), this induced polarization is defined by $\Delta P_{ms} \equiv P_o - P_{eq(0)}$. Since $P_{eq(0)}$ denotes the off-centering (normal) ferroelectric polarization along the polar z-axis or $[001]_h$ under the imposed condition of $\boldsymbol{M} = \boldsymbol{m_1} + \boldsymbol{m_2} = 0$, it does correspond to the Berry-phase polarization[35,36] obtained without imposing any spin structure (i.e., paramagnetic phase). In contrast, P_o represents the net off-centering ferroelectric polarization that includes the exchange coupling effect. Thus, P_o corresponds to the Berry-phase polarization computed by imposing the canted sublattice spin structure with $\boldsymbol{m_1}\cdot\boldsymbol{m_2} = m_o^2\cos\theta = m_o^2\cos(\pi - 2\varphi) = m_o^2\cos(178.6^\circ)$. Since ΔP_{ms} belongs to $\boldsymbol{S}_i\cdot\boldsymbol{S}_j$-type scalar-coupling-induced improper polarization, the computed value of P_o by the Berry-phase method should be independent of the inclusion of spin-orbit coupling effect[22]. Our DFT calculations predict that $\Delta P_{ms} \equiv P_o - P_{eq(0)} = -20\ nC/cm^2$, which indicates $\gamma_q > 0$ according to Eq. (25).

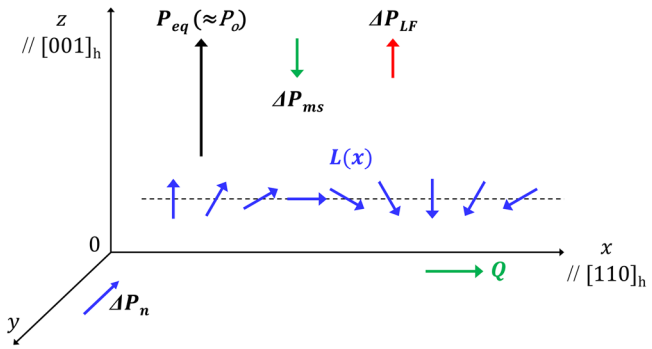

Figure 4. A schematic representation of the off-centering proper ferroelectric polarization, $\boldsymbol{P}_{eq(0)}$, and the three parasitic improper polarizations, $\Delta\boldsymbol{P}_{ms}$, $\Delta\boldsymbol{P}_{LF}$, and $\Delta\boldsymbol{P}_{n}$ in the *R3c* BFO. Among these three improper polarizations, $\Delta\boldsymbol{P}_{LF}$ is parallel to $\boldsymbol{P}_{eq(0)}$ but $\Delta\boldsymbol{P}_{ms}$ is anti-parallel to $\boldsymbol{P}_{eq(0)}$. In contrast, $\Delta\boldsymbol{P}_{n}$ is perpendicular to $\boldsymbol{P}_{eq(0)}$.

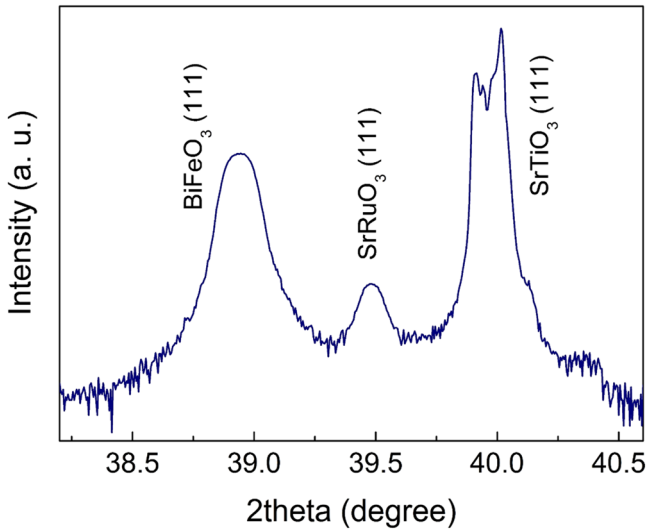

Figure 5. High-resolution theta-2theta x-ray diffraction pattern (XRD) of the $BiFeO_3$(BFO)/$SrRuO_3$/$SrTiO_3$(111) thin-film heterostructure obtained using pulsed laser deposition. As shown, all three layers are characterized by the $[111]_c$-preferential growth. The thicknees of the ferroelectric BFO layer grown along the pseudo-cubic $[111]_c$ is ~400 nm.

Let us estimate the improper polarization (ΔP_{LF}) arising from the Lifshitz gradient coupling. For this, we have to first consider the slowly varying spin reorientation with the periodicity of 620 Å along $[110]_h$ or *x*-axis. The distance between the two neighboring Fe-spin sites along the $[110]_h$ SDW propagation axis is 5.580 Å. Thus, the spin-rotation angle ($\Delta\phi$) between the two neighboring Fe sites in the *x*-*z* plane is given by $\Delta\phi = 360° \times (5.58/620) = 3.24°$. We have imposed the spin-orientation structure and performed *ab initio* calculations by adopting a $2 \times 2 \times 1$ supercell. The estimated *ab initio* value of ΔP_{LF} is ~15 nC/cm^2. However, this computed value is substantially smaller than the experimental value of 36 nC/cm^2 along $[001]_h$[36]. Considering reliability of our *ab initio* value, we will adopt this experimental value in the evaluation of the Lifshitz coupling constant, γ_s, in the next section. We schematically depict these two distinct improper polarizations with their directions in Fig. 4 and these can be summarized by the following ratio: $-\Delta P_{ms}$:$+\Delta P_{LF} = 20{:}36 = 5{:}9$.

Theoretical Estimate of the Three Relevant Coupling Constants. Let us first estimate the biquadratic magnetostrictive coupling constant (γ_q) by exploiting Eq. (25). As estimated in the previous subsection, $\Delta P_{ms} = P_o - P_{eq(0)} = -2.0 \times 10^{-4} C/m^2$. According to our Berry-phase calculations, $P_o = 86.3\ \mu C/cm^2 = 0.863\ C/m^2$. To experimentally check this value, we have fabricated a highly $[111]_c$-oriented 400-nm-thick BFO thin film on the (111)$SrRuO_3$/$SrTiO_3$ substrate [Fig. 5]. As shown in the polarization-electric field (*P*-*E*) hysteresis loop [Fig. 6], the remanent polarization of the $[001]_h$-axis-grown BFO film is ~90 $\mu C/cm^2$, which nearly coincides with the computed value of P_o(=86.3 $\mu C/cm^2$).

As can be deduced from Eq. (17), the invariant for the ferroelectric subsystem is given by $\Delta f_p = \frac{1}{2}\chi_p P^2 + \frac{1}{4}\xi_p P^4 - \gamma_q P^2(\boldsymbol{m_1} \cdot \boldsymbol{m_2}) \approx \frac{1}{2}\chi_p P^2 + \frac{1}{4}\xi_p P^4$ since the biquadratic exchange coupling contribution is negligibly small as compared with the preceding two terms. From this relation, the Landau ϕ^4-expansion

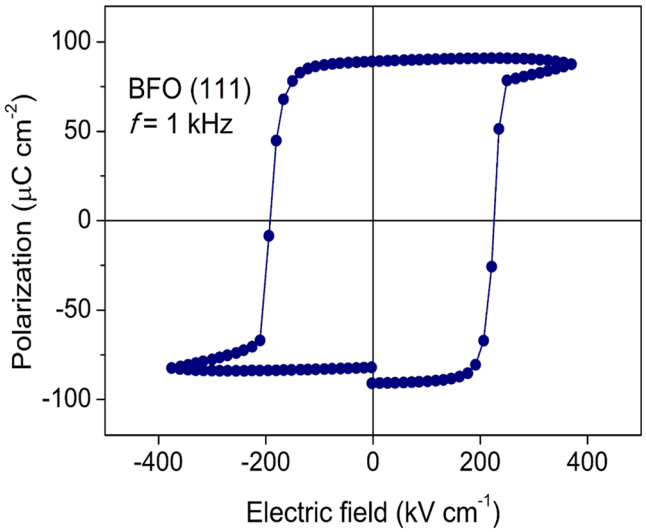

Figure 6. Polarization-electric field ($P-E$) hysteresis loop of the preferential $[111]_c$-oriented BFO film (400-nm-thick) obtained at a measuring frequency of 1 kHz at 300 K. As shown, the net switching polarization ($2P_r$) of the $[111]_c$-preferentially grown BFO film is ~180 $\mu C/cm^2$, which indicates that the remanent polarization (P_r) is ~90 $\mu C/cm^2$. According to the XRD pattern (Fig. 5), the in-plane film strain in the $[111]_c$-oriented BFO layer is fully relaxed at the thickness of 400 nm. Thus, the measured P_r value (~90 $\mu C/cm^2$) can be treated as a bulk P_r value of the *R3c* BFO.

coefficient ξ_p can be derived in terms of P_{eq} and $(\Delta f_p)_{eq}$, where $\left(\Delta f_p\right)_{eq}$ denotes the equilibrium free-energy density of the ferroelectric subsystem with respect to that of the paraelectric reference system. This can be written explicitly as

$$\xi_p = -4\left(\Delta f_p\right)_{eq} \cdot \left(P_{eq}\right)^{-4} \tag{36}$$

where $(P_{eq})^2 = -\chi_p/\xi_p$. On the other hand, $P_{eq}(=P_o) = 0.863\ C/m^2$. According to the *ab initio* calculations[17], $\left(\Delta f_p\right)_{eq} = -0.381\ eV$ per hexagonal cell containing six BFO formula cells ($a = 5.57987$ Å, $c = 13.87229$ Å), which is equivalent to $-0.163 \times 10^{+9}\ J/m^3$. Plugging these two values into Eq. (36), one finds that $\xi_p = +1.175 \times 10^{+9}\ (J \cdot m^5/C^4)$. On the other hand, $m_o \approx 5\mu_B = 4.637 \times 10^{-23}\ (J \cdot T^{-1})$ for the high-spin Fe^{3+} in the *R3c* $BiFeO_3$ (ref.[2]). In addition, $|\cos\theta| = |\cos(\pi - 2\varphi)| = |\cos(178.6°)| \approx 1$. Using all these values and rewriting Eq. (25) in terms of γ_q, we obtain

$$\gamma_q = \frac{-\xi_p P_o\left\{P_o - P_{eq(o)}\right\}}{m_o^2} = +9.43 \times 10^{+49}\ (m \cdot T^2/J \cdot C^2) \tag{37}$$

To estimate the Lifshitz exchange-coupling constant (γ_s), we have reconsidered Eq. (24). As mentioned previously, we have adopted the experimental value of $3.6 \times 10^{-4}\ (C/m^2)$ as ΔP_{LF}. In addition to this, we use the following values for the estimate of γ_s: $P_o = 0.863\ (C/m^2)$, $\xi_p = +1.175 \times 10^{+9}\ (J \cdot m^5/C^4)$, $Q = 2\pi/\lambda = 1.013 \times 10^{+8}\ (m^{-1})$, and $L_o^2 = 4m_o^2\cos^2\varphi \approx 4m_o^2$ with $m_o = 4.637 \times 10^{-23}\ (J \cdot T^{-1})$. Using these five values and rewriting Eq. (24) in terms of γ_s, we obtain

$$\gamma_s = \frac{-2\,\xi_p P_o^2 \Delta P_{LF}}{L_o^2\, Q} = -7.23 \times 10^{+41}\ (T^2/J \cdot C) \tag{38}$$

As discussed previously, a negative sign of γ_s indicates that the cycloidal spin ordering is formed spontaneously in the unstrained *R3c* BFO. Let us now estimate d_{DM}, a measure of the reverse DM interaction, using Eq. (27). Then, plugging $P_o = 0.863\ (C/m^2)$, $\xi_p = +1.175 \times 10^{+9}(J \cdot m^5/C^4)$, $\lambda = 620$ Å, $\Delta\varphi = 3.24°$, $\varphi = 0.7°$, and $\gamma_s = -7.23 \times 10^{+41}(T^2/J \cdot C)$ into Eq. (27), we obtain $d_{DM} = +4.98 \times 10^{+44}(T^2/J \cdot V \cdot m^2)$.

Having estimated d_{DM}, we are now ready to examine our previous proposition that the y-component value of the reverse DM coupling-induced polarization [$\equiv\Delta P_{DM}(y)$ or ΔP_n] is relatively negligible as compared with the corresponding z-component value [$\equiv\Delta P_{DM}(z)$] (See, the previous section of 'Improper Polarization and Invariant caused by the Reverse DM Interaction'). According to Eq. (4), the ratio of the two perpendicular improper polarizations can be written as

$$\frac{\Delta P_{DM}(y)}{\Delta P_{DM}(z)} = \frac{m_y\{1 - \cos(\Delta\varphi)\}}{m_o d_{DM} \sin\varphi \sin(\Delta\varphi)} \tag{39}$$

We used the following values to estimate the above ratio: $\Delta\varphi = 3.24°$, $\varphi = 0.7°$, $d_{DM} = +4.98 \times 10^{+44}(T^2/J \cdot V \cdot m^2)$, and $(m_y/m_o) = \sin(\chi)$, where χ denotes the y-component spin-canting angle along the x-axis. In contrast, φ designates the x-component spin-canting angle along the z-axis [Fig. 2]. According to our previous *ab initio* calculations[17], $\chi = 0.203°$ along the x-axis, $[110]_h$. Plugging all these values into Eq. (39), one obtains that $\Delta P_{DM}(y)/\Delta P_{DM}(z)$ is as small as 1.65×10^{-47}. This clearly justifies our previous proposition that the y-component value of the reverse DM coupling-induced polarization is completely negligible as compared with the corresponding z-component value.

Release of the Latent Magnetization in a Constrained Thin Film. According to the study of Bai and co-workers[37], the epitaxial film-constraint induces the destruction of a spatially modulated cycloidal spin structure in the bulk *R3c* BFO, releasing a latent AFM component locked within the cycloid. This corresponds to a transition from the incommensurately modulated cycloidal spin state to the homogeneously canted spin state in a constrained film with the onset thickness of ~150 nm[38]. Ryu and co-workers[38] further showed that the release of a latent AFM magnetization associated with the transition to the homogeneous spin state accompanies with a pronounced increase in the magnetic susceptibility (χ_m) in epitaxially constrained BFO thin films. We will quantitatively account for these observations by using Eq. (34). For an epitaxially constrained thin film having a homogeneous spin structure, we impose that $\gamma_s = 0$ and $\kappa_G = 0$ by considering the disappearance of a spatially modulated cycloidal spin structure[39]. For a constrained epitaxial thin film, Eq. (34) thus reads:

$$\left(M_{eq(f)}\right)^2 = \left(M_{eq(0)}\right)^2 + 4\delta(\boldsymbol{m_1} \cdot \boldsymbol{m_2})_{eq,f} - \left(\gamma_q P^2/2\xi_l\right),$$

where $M_{eq(f)}$ denotes the equilibrium magnetic remanence of the constrained epitaxial film. On the other hand, $M_{eq(0)}$ denotes the equilibrium magnetic remanence in the absence of any ME coupling. Thus, $\left(M_{eq(0)}\right)^2 \equiv -\chi_m/\xi_m$. Using this relation and Eq. (34) for $M_{eq(b)}$, one can derive the following relation for the latent magnetization released by the transition to the homogeneously canted spin state in a constrained film:

$$\Delta M_{eq} \equiv M_{eq(f)} - M_{eq(b)} = \frac{2\{\gamma_s PQ + \kappa_G Q^2\}}{\xi_l \{M_{eq(f)} + M_{eq(b)}\}} \approx \frac{\{-|\gamma_s|PQ + \kappa_G Q^2\}}{\xi_l M_{eq(b)}} > 0 \tag{40}$$

where $M_{eq(b)}$ denotes the equilibrium magnetic remanence of the bulk *R3c* BFO and $\gamma_s < 0$. In obtaining Eq. (40) we used the following equality:

$$\begin{aligned}\left\{4\delta(\boldsymbol{m_1} \cdot \boldsymbol{m_2})_{eq,f} - 4\delta(\boldsymbol{m_1} \cdot \boldsymbol{m_2})_{eq,b}\right\} &= 4\left\{(\boldsymbol{m_1} \cdot \boldsymbol{m_2})_{eq,f} - (\boldsymbol{m_1} \cdot \boldsymbol{m_2})_{eq,b}\right\} \\ &= 4m_o^2\{\cos\theta_f - \cos\theta_b\} \approx 0,\end{aligned}$$

where the AFM spin angle of the bulk *R3c* BFO (θ_b) is essentially unaffected by the formation of a constrained thin film, namely, $\theta_f = \theta_b = 180° - 2\varphi = 178.6°$. The inequality sign in Eq. (40) reflects the observation associated with the transition to the homogeneously canted spin state in a constrained epitaxial film.

One can readily obtain the following inequality by considering the right-hand-side of Eq. (40): $k_G \geq \frac{|\gamma_s|P}{Q}$. Thus, the lower limit of the Ginzburg gradient-energy coefficient $[(\kappa_G)_{ll}]$ can be estimated by using $(k_G)_{l.l.} = \frac{|\gamma_s|P}{Q}$. Plugging the previously estimated values of γ_s, P and Q into this lower limit, we obtain $(\kappa_G)_{l.l.} = 6.16 \times 10^{+33}\ (T^2/J \cdot m)$. Thus, we have estimated all four coupling constants needed for the Landau-Lifshitz-Ginzburg treatment of the *R3c* BFO.

The saturation magnetization (M_s) or magnetic susceptibility (χ_M), in general, can be readily estimated from the *M-H* hysteresis curve. On the contrary, ΔM_{eq} is too small[30,38] to quantitatively discuss this effect in terms of γ_s and κ_G. Thus, we have examined a variation in χ_M. In doing this, we first consider the thermodynamic potential of the AFM subsystem. One can write the following relation by exploiting Eq. (17) for $\Delta f(L)$, Eq. (13) for the Lifshitz invariant, and Eq. (35) for the Ginzburg gradient term:

$$\Delta f(L) = +\frac{1}{2}\chi_l L^2 + \frac{1}{4}\xi_l L^4 - \frac{1}{4}\gamma_q P^2(M^2 - L^2) + \frac{1}{2}\kappa_G L^2 Q^2 + \gamma_s P L^2 Q \tag{41}$$

where $L^2 = M^2 - 4(\boldsymbol{m_1} \cdot \boldsymbol{m_2}) = M^2 - 4m_o^2\cos\theta > M^2$. Plugging this result into Eq. (41) and adding the term, $-\boldsymbol{H} \cdot \boldsymbol{M}$, to Eq. (41), one can obtain the free-energy functional $[\Delta f_H(M, \theta)]$ under an external magnetic field, $\boldsymbol{H}$. Taking the dynamic equilibrium condition, i.e., $(\partial \Delta f_H(M, \theta)/\partial M)_{P,\theta} = 0$, one can eventually derive the following relation for the inverse magnetic susceptibility:

$$\frac{1}{\chi_M} \equiv \left(\frac{\partial H}{\partial M}\right)_{P,\theta} = \{\chi_l + 3\xi_l M^2 + 4\xi_l m_o^2|\cos\theta| + (2\gamma_s PQ + \kappa_G Q^2)\} \tag{42}$$

The term inside a small bracket, $2\gamma_s PQ + \kappa_G Q^2$, is non-zero for a bulk crystal but is zero for a constrained epitaxial film. If this term is positive, the inverse susceptibility decreases or equivalently, M_s increases upon the transition to the homogeneous spin state in a constrained epitaxial film. On the contrary, the reverse is true if this term is

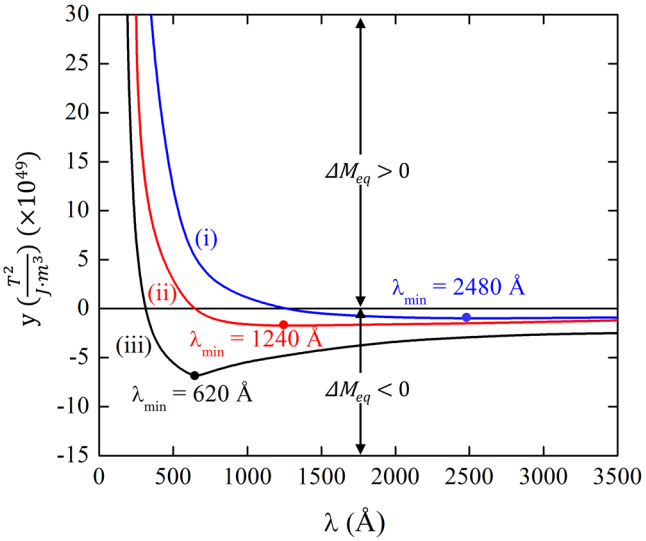

Figure 7. Plotting the computed y value, which is a measure of $\Delta \boldsymbol{M}_{eq}$ as a function of the wavelength (λ) of SDW. The κ_G and $|\gamma_s|$ values corresponding to the three computed curves are: (**i**) $|\gamma_s| = 7.23 \times 10^{+41}\,(T^2/J \cdot C)$ and $\kappa_G = 2(\kappa_G)_{l.l.} = 12.32 \times 10^{+33}\,(T^2/J \cdot m)$, (**ii**) $|\gamma_s| = 7.23 \times 10^{+41}(T^2/J \cdot C)$ and $\kappa_G = (\kappa_G)_{l.l.} = 6.16 \times 10^{+33}\,(T^2/J \cdot m)$, (**iii**) $|\gamma'_s| = 2|\gamma_s| = 14.46 \times 10^{+41}\,(T^2/J \cdot C)$ and $\kappa_G = (\kappa_G)_{l.l.} = 6.16 \times 10^{+33}\,(T^2/J \cdot m)$. The same polarization (P) value of 0.863 (C/m^2) was used for all three curves. For given κ_G and $|\gamma_s|$ values, there exists a certain critical value of λ below which $\Delta M_{eq} > 0$, or equivalently, the latent magnetization is released upon the transition to the homogeneously canted spin state in an epitaxially constrained film. The three critical λ_c values are 1240 Å, 620 Å, and 310 Å for the curve (**i**), (**ii**), and (**iii**), respectively.

negative. According to the experimental observation of χ_m[38], the former is true. In other words, $2\gamma_s PQ + \kappa_G Q^2 > 0$, or equivalently, $|\gamma_s| < \frac{k_G Q}{2P}$.

According to Eq. (40), the enhanced magnetic remanence associated with the formation of epitaxially constrained film (ΔM_{eq}) is determined by two material parameters, γ_s and κ_G. We thus have examined the effects of these two parameters on ΔM_{eq} as a function of the wavelength (λ) of cycloidal SDW. In doing this, we have multiplied ΔM_{eq} by $\xi_l M_{eq(b)}$ since ΔM_{eq} itself is too small to be experimentally evaluated. Thus, Eq. (40) is rearranged as

$$y \equiv \left\{\xi_l M_{eq(b)}\right\} \cdot \Delta M_{eq} = +\kappa_G Q^2 - |\gamma_s| PQ = \frac{4\pi^2 \kappa_G}{\lambda^2} - \frac{2\pi |\gamma_s| P}{\lambda} \tag{43}$$

Thus, y is a measure of the enhanced magnetic remanence upon the transition to the homogeneous canted spin state in a constrained thin film. As shown in Fig. 7, y decreases rapidly with increasing λ value and reaches its characteristic minimum value, which is regardless of $|\gamma_s|$ or κ_G value. According to Eq. (43), y reaches its minimum at $\lambda_{min} = \frac{4\pi k_G}{|\gamma_s| P}$, explaining the computed result shown in Fig. 7. The characteristic minimum y value is $y_{min} = -\frac{|\gamma_s|^2 P^2}{4k_G} < 0$. Thus, the magnitude of y_{min} is proportional to the square of $|\gamma_s|$ but is inversely proportional to κ_G. This prediction is graphically illustrated in Fig. 7. Equation (43) further predicts that y becomes *0* at $\lambda_c = \frac{2\pi k_G}{|\gamma_s| P}$, which is regardless of $|\gamma_s|$. Thus, the critical value λ_c corresponding to $(\kappa_G)_{l.l.}$ (i.e., lower limit of κ_G) can be deduced by plugging $\kappa_G = \frac{|\gamma_s| P}{Q} = 6.16 \times 10^{+33}(T^2/J \cdot m)$ into $\lambda_c = \frac{2\pi k_G}{|\gamma_s| P}$, yielding $\lambda_c = 620$ Å. This λ_c value corresponds to the curve (ii) in Fig. 7. In case of the *R3c* BFO, only the region with $y \geq 0$ is experimentally meaningful since the release of the latent magnetization is observed upon the transition to the homogeneously canted spin state in epitaxially constrained BFO thin films. As shown in Fig. 7, λ should be smaller than a certain critical value for $\Delta M_{eq} > 0$ (i.e., for $y \geq 0$). Since $\lambda_c = \frac{2\pi k_G}{|\gamma_s| P}$, this critical λ_c value increases with κ_G but decreases with increasing value of $|\gamma_s|$.

Conclusion

We have theoretically identified the three free-energy invariants (Δf_{LF}, Δf_{ms}, Δf_G) that are closely related to the manifestation of the two distinct spin-coupling-induced improper polarizations by suitably exploiting the Landau-Lifshitz-Ginzburg thermodynamic potential for the *R3c* BFO. The two relevant parasitic improper polarizations are: (i) $\Delta \boldsymbol{P}_{LF}$ arising from the Lifshitz gradient coupling, which can be equated with the improper polarization caused by the reverse DM interaction, $\Delta \boldsymbol{P}_{DM}$, and (ii) $\Delta \boldsymbol{P}_{ms}$ originating from the magnetostrictive interaction. The two improper polarizations are comparable in their magnitudes (20 *vs.* 36 nC/cm^2). The direction of the off-centering proper ferroelectric polarization ($\boldsymbol{P}_{eq(0)}$) is parallel to $\Delta \boldsymbol{P}_{LF}$ while it is antiparallel to $\Delta \boldsymbol{P}_{ms}$. We

have further predicted that the magnetic susceptibility (χ_m) increases substantially upon the transition to the homogeneous spin state in a constrained epitaxial BFO film, which accounts for the experimental observation well.

Computational Methods

To obtain material parameters needed to quantitatively estimate three distinct polarizations and coupling constants, we have performed first-principles DFT calculations on the basis of the generalized gradient approximation (GGA)[40] and the GGA+U method[41] implemented with the projector augmented-wave (PAW) method[42] using the Vienna *ab initio* simulation package (VASP)[43,44]. The Hubbard U_{eff} of 4.5 eV was chosen on the basis of empirical corrections. We explicitly treated five valence electrons for Bi ($6s^26p^3$), eight for Fe ($3d^64s^2$), and six for oxygen ($2s^22p^4$). Actual DFT calculations were performed using (i) a $4 \times 4 \times 3$ Monkhorst-Pack $\boldsymbol{k}$-point mesh[45] centered at Γ for the *R3c* structure, (ii) a 500 eV plane-wave cutoff, and (iii) the tetrahedron method with the Blöchl corrections for the Brillouin-zone integrations[46]. Structural optimizations were basically performed for the 30-atoms cell which corresponds to a hexagonal unit cell. In contrast, we adopted a $2 \times 2 \times 1$ hexagonal supercell (containing 4 unit cells) to evaluate ΔP_{LF}. The ions were relaxed until the Hellmann-Feynman forces on them were less than 0.01 eV/Å.

References

1. Hill, N. A. Why are there so few magnetic ferroelectrics? *J. Phys. Chem. B* **104**, 6694 (2000).
2. Dong, S., Liu, J.-M., Cheong, S.-W. & Ren, Z. Multiferroic materials and magnetoelectric physics: symmetry, entanglement, excitation, and topology. *Advances in Physics* **64**, 519–626 (2015).
3. Tsymbal, E. Y. & Kohlstedt, H. Tunneling across a ferroelectric. *Science* **313**, 181–183 (2006).
4. Ramesh, R. & Spaldin, N. A. Multiferroics: progress and prospects in thin films. *Nat. Mater.* **6**, 21–29 (2007).
5. Scott, J. F. Data Storage: Multiferroic memories. *Nat. Mater.* **6**, 256–257 (2007).
6. Catalan, G. & Scott, J. F. Physics and applications of bismuth ferrite. *Adv. Mater.* **21**, 2463–2485 (2009).
7. Tokura, Y. & Seki, S. Multiferroics with spiral spin orders. *Adv. Mater.* **22**, 1554–1565 (2010).
8. Ma, J., Hu, J., Li, Z. & Nan, C.-W. Recent progress in multiferroic magnetoelectric composites: From bulk to thin films. *Adv. Mater.* **23**, 1062–1087 (2011).
9. Nechache, R. *et al*. Bandgap tuning of multiferroic oxide solar cells. *Nat. Photonics* **9**, 61–67 (2015).
10. Kubel, F. & Schmid, H. Structure of a ferroelectric and ferroelastic monodomain crystal of the perovskite $BiFeO_3$. *Acta Crystallogr., Sect. B: Struct. Sci.* **46**, 698–702 (1990).
11. Fischer, P., Polomska, M., Sosnowska, I. & Szymanski, M. Temperature dependence of the crystal and magnetic structures of $BiFeO_3$. *J. Phys. C* **13**, 1931–1940 (1980).
12. Ruette, B. *et al*. Magnetic-field-induced phase transition in $BiFeO_3$ observed by high-field electron spin resonance: Cycloidal to homogeneous spin order. *Phys. Rev. B: Condens. Matter Mater. Phys.* **69**, 064114 (2004).
13. Lebeugle, D., Colson, D., Forget, A. & Viret, M. Very large spontaneous electric polarization in $BiFeO_3$ single crystals at room temperature and its evolution under cycling fields. *Appl. Phys. Lett.* **91**, 022907 (2007).
14. Neaton, J. B., Ederer, C., Waghmare, U. V., Spaldin, N. A. & Rabe, K. M. First-principles study of spontaneous polarization in multiferroic $BiFeO_3$. *Phys. Rev. B: Condens. Matter Mater. Phys.* **71**, 014113 (2005).
15. Ederer, C. & Spaldin, N. A. Effect of epitaxial strain on the spontaneous polarization of thin film ferroelectrics. *Phys. Rev. Lett.* **95**, 257601 (2005).
16. Ravindran, P., Vidya, R., Kjekshus, A., Fjellvåg, H. & Eriksson, O. Theoretical investigation of magnetoelectric behavior in $BiFeO_3$. *Phys. Rev. B: Condens. Matter Mater. Phys.* **74**, 224412 (2006).
17. Lee, J.-H. *et al*. Variations of ferroelectric off-centering distortion and 3*d*-4*p* orbital mixing in La-doped $BiFeO_3$ multiferroics. *Phys. Rev. B: Condens. Matter Mater. Phys.* **82**, 045113 (2010).
18. Sosnowska, I., Peterlin-Neumaier, T. & Steichele, E. Spiral magnetic ordering in bismuth ferrite. *J. Phys. C* **15**, 4835–4846 (1982).
19. Lebeugle, D. *et al*. Electric-field-induced spin flop in $BiFeO_3$ single crystal at room temperature. *Phys. Rev. Lett.* **100**, 227602 (2008).
20. Saenrang, W. *et al*. Deterministic and robust room-temperature exchange coupling in monodomain multiferroic $BiFeO_3$ heterostructure. *Nature Commun.* **8**, 1583 (2017).
21. Katsura, H., Nagaosa, N. & Balatsky, A. V. Spin current and magnetoelectric effect in noncollinear magnets. *Phys. Rev. Lett.* **95**, 057205 (2005).
22. Malashevich, A. & Vanderbilt, D. First principles study of improper ferroelectricity in $TbMnO_3$. *Phys. Rev. Lett.* **101**, 037210 (2008).
23. Shi, X. X., Liu, X. Q. & Chen, X. M. Readdressing of magnetoelectric effect in bulk $BiFeO_3$. *Adv. Func. Mater.* **27**, 1604037 (2017).
24. de Sousa, R. & Moore, J. E. Optical coupling to spin waves in the cycloidal multiferroic $BiFeO_3$. *Phys. Rev. B: Condens. Matter Mater. Phys.* **77**, 012406 (2008).
25. Lee, S. *et al*. Negative magnetostrictive magnetoelectric coupling of $BiFeO_3$. *Phys. Rev. B: Condens. Matter Mater. Phys.* **88**(R), 060103 (2013).
26. Sparavigna, A. Role of Lifshitz invariants in liquid crystals. *Materials* **2**, 674–698 (2009).
27. Devonshire, A. F. Theory of barium titanate: Part I. *Philos. Mag.* **40**, 1040–1063 (1949).
28. Amin, A., Newnham, R. E. & Cross, L. E. Effect of elastic boundary conditions on morphotropic $Pb(Zr,Ti)O_3$ piezoelectrics. *Phys. Rev. B: Condens. Matter Mater. Phys.* **34**, 1595–1598 (1986).
29. Oh, S. H. & Jang, H. M. Two-dimensional thermodynamic theory of epitaxial $Pb(Zr,Ti)O_3$ thin films. *Phys. Rev. B: Condens. Matter Mater. Phys.* **62**, 14757–14765 (2000).
30. Sosnowska, I. & Zvezdin, A. K. Origin of the long period magnetic ordering in $BiFeO_3$. *J. Magn. Magn. Mater.* **140–144**, 167–168 (1995).
31. de Sousa, R. & Moore, J. E. Electrical control of magnon propagation in multiferroic $BiFeO_3$ films. *Appl. Phys. Lett.* **92**, 022514 (2008).
32. Park, J.-G., Le, M. D., Jeong, J. & Lee, S. Structure and spin dynamics of multiferroic $BiFeO_3$. *J. Phys.: Condens. Matter* **26**, 433202 (2014).
33. Mostovoy, M. Ferroelectricity in spiral magnets. *Phys. Rev. Lett.* **96**, 067601 (2008).
34. Tokunaga, M., Azuma, M. & Shimakawa, Y. High-field study of strong magnetoelectric coupling in single-domain crystals of $BiFeO_3$. *J. Phys. Soc. Jpn.* **79**, 064713 (2010).
35. King-Smith, R. D. & Vanderbilt, D. Theory of polarization of crystalline solids. *Phys. Rev. B: Condens. Matter Mater. Phys.* **47**(R), 1651 (1993).
36. Vanderbilt, D. & King-Smith, R. D. Electric polarization as a bulk quantity and its relation to surface charge. *Phys. Rev. B: Condens. Matter Mater. Phys.* **48**, 4442 (1993).

37. Bai, F. *et al.* Destruction of spin cycloid in $(111)_c$-oriented $BiFeO_3$ thin films by epitaxial constraint: Enhanced polarization and release of latent magnetization. *Appl. Phys. Lett.* **86**, 032511 (2005).
38. Ryu, S. *et al.* Enhanced magnetization and modulated orbital hybridization in epitaxially constrained $BiFeO_3$ thin films with rhombohedral symmetry. *Chem. Mater.* **21**, 5050–5057 (2009).
39. Bea, H., Bibes, M., Petit, S., Kreisel, J. & Barthelemy, A. Structural distortion and magnetism of $BiFeO_3$ epitaxial thin films: a Raman spectroscopy and neutron diffraction study. *Phil. Mag. Lett.* **87**, 165–174 (2007).
40. Perdew, J. P., Burke, K. & Wang, Y. Generalized gradient approximation for the exchange-correlation hole of a many-electron system. *Phys. Rev. B: Condens. Matter Mater. Phys.* **54**, 16533 (1996).
41. Anisimov, V. I., Aryasetiawan, F. & Liechtenstein, A. I. First-principles calculations of the electronic structure and spectra of strongly correlated systems: the LDA+U method. *J. Phys.: Condens. Matter* **9**, 767–808 (1997).
42. Blöchl, P. E. Projector augmented-wave method. *Phys. Rev. B: Condens. Matter Mater. Phys.* **50**, 17953–17979 (1994).
43. Kresse, G. & Furthmůller, J. Efficient iterative schemes for *ab initio* total-energy calculation using a plane-wave basis set. *Phys. Rev. B: Condens. Matter Mater. Phys.* **54**, 11169–11186 (1996).
44. Kresse, G. & Joubert, D. From ultrasoft pseudopotentials to the projector augmented-wave method. *Phys. Rev. B: Condens, Matter Mater. Phys.* **59**, 1758–1775 (1999).
45. Monkhorst, H. J. & Pack, J. D. Special point for Brillouin-zone integrations. *Phys. Rev. B: Condens, Matter Mater. Phys.* **13**, 5188–5192 (1976).
46. Blöchl, P. E., Jepsen, O. & Andersen, O. K. Improved tetrahedron method for Brillouin-zone integrations. *Phys. Rev. B: Condens, Matter Mater. Phys.* **49**, 16223–16233 (1994).

Acknowledgements

This work was supported by the Basic Science Research Program (Grant No. 2016R 1D1A1B 03933253) through the National Research Foundation (NRF) of Republic of Korea.

Author Contributions

H.M.J. derived LLG formalisms and did theoretical analysis. H.H. fabricated BFO thin films and performed dielectric/structural measurements. J.-H.L. did *ab initio* calculations. H.M.J. wrote the manuscript. All authors read and commented on the manuscript.

Additional Information

Competing Interests: The authors declare that they have no competing interests.

Publisher's note: Springer Nature remains neutral with regard to jurisdictional claims in published maps and institutional affiliations.